

# A Neutron Scattering Study of the $H$ - $T$ Phase Diagram of the Bond Frustrated Magnet $\text{ZnCr}_2\text{S}_4$

D. Hsieh,<sup>1,2</sup> Y. W. Li,<sup>1</sup> S. Watauchi,<sup>3</sup> Chang Liu,<sup>1</sup> Q. Huang,<sup>4</sup> J. W. Lynn,<sup>4</sup> R. J. Cava,<sup>3</sup> and M. Z. Hasan<sup>1</sup>

<sup>1</sup>*Joseph Henry Laboratories of Physics, Princeton University, Princeton, New Jersey 08544, USA*

<sup>2</sup>*(Present Address) Institute for Quantum Information and Matter, California Institute of Technology, Pasadena, California 91125, USA*

<sup>3</sup>*Department of Chemistry, Princeton University, Princeton, New Jersey 08544, USA*

<sup>4</sup>*NIST Center for Neutron Research, Gaithersburg, Maryland 20899, USA*

(Dated: June 3, 2014)

Detailed neutron scattering measurements on the bond frustrated magnet  $\text{ZnCr}_2\text{S}_4$  reveal a rich  $H$ - $T$  phase diagram. The field dependence of the two subsequent antiferromagnetic transitions follows closely that of recently reported structural instabilities, providing further evidence for spin driven Jahn-Teller physics. The incommensurate helical ordered phase below  $T_{N1} = 15.5$  K exhibits gapless spin wave excitations, whereas a spin wave gap  $\Delta \simeq 2$  meV opens below  $T_{N2} = 8$  K as the system undergoes a first-order transition to a commensurate collinear ordered phase. The spin wave gap is closed by a strong magnetic field.

PACS numbers: 75.25.+z, 73.20.At, 71.20.-b

Strong geometrical frustration is consistently being found in magnetic  $B$ -site spinel oxides  $AB_2X_4$  ( $X=\text{O}$ ) [1–6]. These systems are characterized by Heisenberg spins on a lattice of corner sharing tetrahedra interacting via antiferromagnetic (AFM) nearest-neighbor direct exchange. In the spinel chalcogenides ( $X=\text{S}, \text{Se}$ ) on the other hand, the nearest-neighbor direct exchange is weakened due to a larger  $B$ - $B$  distance and the small ferromagnetic (FM) Cr-S-Cr superexchange becomes the dominant interaction between them. Nevertheless the spins often remain frustrated because competing further neighbor exchanges become important [7–10]. Strong spin-phonon coupling plays a major role in relieving both geometrical and bond frustration in these systems, manifested by both uniform and nonuniform lattice distortions that commonly accompany the magnetic ordering [11, 12]. Characterizing these distortions in bond frustrated spinels is particularly crucial in light of their recently discovered novel magnetoelectric properties [13–15]. While the structural distortions involved are small and largely nonuniform, thus making them difficult to detect using standard diffraction techniques, its effect on system dynamic variables such as phonons and magnons can be clearly measured.

The correlated insulator  $\text{ZnCr}_2\text{S}_4$  is a strongly bond frustrated material (the value of the frustration parameter  $f = |\Theta_{CW}|/T_N \simeq 0.5$ ). Hamedoun *et al.* performed neutron diffraction measurements in zero magnetic field and reported the following results [16]. At  $T_{N1}=15.5$  K, the material undergoes a second order phase transition from a paramagnetic to a helical ordered phase. The helical structure is characterized by an incommensurate ordering wave vector  $\vec{k}_1=(0\ 0\ 0.79)$  with spins confined and ferromagnetically ordered within the (001) planes. Below  $T_{N2}=8$  K, the helical structure partially transforms into two collinear commensurate structures with  $\vec{k}_2=(\frac{1}{2}\frac{1}{2}0)$  and  $\vec{k}_3=(1\frac{1}{2}0)$  with spins oriented parallel to the [110] and [001] directions respectively. More recently,

specific heat, thermal expansion and phonon anomalies have been reported at both  $T_{N1}$  and  $T_{N2}$ , and an external magnetic field has been found to suppress only the anomalies at  $T_{N2}$  [8]. These results suggest that the helical structure is stabilized over the collinear structures in a field, and that spin-phonon coupling may be driving structural distortions at both  $T_{N1}$  and  $T_{N2}$  that have so far not been resolved. In this Letter, we use neutron scattering to study the magnetic field dependence of both the spin order and dynamics of  $\text{ZnCr}_2\text{S}_4$  for the first time. Our results show that the magnetic order parameters display the same field dependence as the reported structural anomalies do, providing stronger support for spin-driven structural instabilities at both  $T_{N1}$  and  $T_{N2}$ .

A 10 g powder sample of  $\text{ZnCr}_2\text{S}_4$  was prepared by solid state reaction between stoichiometric amounts of ZnS, Cr and S. Rietveld refinement of neutron diffraction data from the NIST Center for Neutron Research BT-1 diffractometer showed that the sample is single phase spinel with space group  $Fd\bar{3}m$  with lattice parameter  $a=9.986$  Å and sulphur fractional coordinate  $u=0.385$  for  $T=300$  K. Magnetic properties were measured using a commercial SQUID magnetometer (Quantum Design MPMS-5). Neutron diffraction scans were performed at NIST on the thermal-neutron triple-axis spectrometer BT-7 using a fixed incident and final energy of 14.7 meV [17]. We used PG(002) reflections for both the monochromator and the analyzer which was operated in flat mode, and used horizontal beam collimations of open-50'-50'-open. Elastic and inelastic neutron scattering measurements were performed on the cold neutron time-of-flight spectrometer (DCS) using 3 Å and 4.8 Å incident neutrons. All magnetic fields were applied perpendicular to the scattering plane. We used the integrated intensity of several nuclear Bragg peaks to determine the normalized magnetic neutron scattering intensity [18]

$$\tilde{I}(Q, \omega) = \int \frac{d\Omega_{\hat{Q}}}{4\pi} \left| \frac{g}{2} F(Q) \right|^2 \times \sum_{\alpha\beta} (\delta_{\alpha\beta} - \hat{Q}_{\alpha} \hat{Q}_{\beta}) S^{\alpha\beta}(\vec{Q}, \omega) \quad (1)$$

where  $F(Q)$  is the magnetic form factor for  $\text{Cr}^{3+}$ ,  $S^{\alpha\beta}(\vec{Q}, \omega)$  is the dynamic spin correlation function and  $g$  is the Landé  $g$ -factor. Error bars where indicated are statistical in origin and represent one standard deviation.

Figures 1(a)- 1(c) are color images of  $\tilde{I}(Q, \omega)$  at three temperatures. In the paramagnetic phase, Fig.1(c) shows evidence for critical fluctuations of small helically correlated clusters. Here, the static spin correlation length  $\xi$  is close to the Cr-Cr separation as determined by neutron diffraction. Strong fluctuations of small AFM clusters at  $T \gg T_N$  is also a hallmark of geometrically frustrated magnets. At  $T=12$  K, in the long-range helical ordered phase, rather well defined spin wave excitations appear (Figs.1(b) and (e)) whose energy tends to zero at the magnetic Brillouin zone center  $k_1$ , and reaches a zone boundary energy near 1.5 meV at  $Q \sim 0.3 \text{ \AA}^{-1}$ . By subtracting the nuclear incoherent scattering from  $\tilde{I}(Q, \omega)$  and integrating over  $\hbar\omega$  and  $Q$ , we obtained the sum rule  $S(S+1)=3.8(3)$  at 12 K, which is the expected value of  $15/4 = 3.75$  for orbitally-quenched  $\text{Cr}^{3+}$  ( $S=3/2$ ) ions. This and the  $Q$  dependence tell us that the scattering is magnetic. By integrating the 12 K data over  $\hbar\omega \in [0.5, 3]\text{meV}$  and  $Q \in [0.2, 1]\text{\AA}^{-1}$  we obtain the total fluctuating moment  $\langle \delta m \rangle^2 = (3/2) \int \hbar d\omega \int Q^2 dQ [\tilde{I}(Q, \hbar\omega) / |F(Q)|^2] / \int Q^2 dQ = 1.20(3)/\text{Cr}$ , which is considerably less than that found in  $\text{ZnCr}_2\text{O}_4$  at the lowest temperatures [19]. For  $T < T_{N2}$  (Fig. 1(a)),  $\langle \delta m \rangle^2$  decreases slightly to  $0.96(7)/\text{Cr}$ , but nearly half of this spectral weight shifts to higher energies between 2–3 meV. Figure 1(f) shows the energy dependence of the magnetic scattering at  $Q=0.45 \text{ \AA}^{-1}$  averaged over an  $0.3 \text{ \AA}^{-1}$  interval. Even below  $T_{N2}$ , intensity continues to be transferred from a low energy maximum centered about 1 meV to a high energy maximum centered around 2.5 meV. This and the difference of the  $T=1.5$  K and  $T=12$  K spectra (Fig. 1(d)) strongly suggest that the low energy scattering is due to remnant helically ordered regions of the sample. The excitations intrinsic to the collinear phase are seen to be gapped by approximately 2 meV and disperse with a bandwidth ( $\sim 1.5$  meV) close to that observed in the helical phase. The latter fact indicates that any structural distortion occurring at  $T_{N2}$  does not alter the exchange constants significantly. However the origin of the gap is unclear, one possibility being some single-ion anisotropy that develops via a local distortion of the Cr-S octahedra. Alternatively, more exotic scenarios such as a lifted local resonance mode [19] may be at play.

We proceed to study the magnetic field dependence of the phase boundary between the ordered magnetic states.

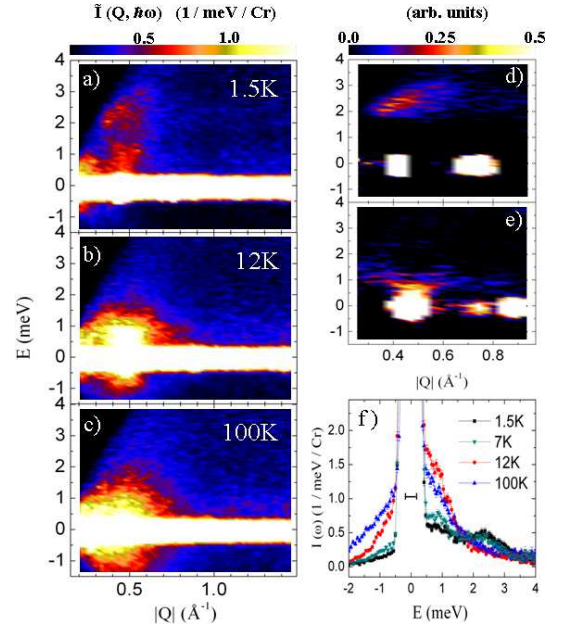


FIG. 1: **Zero field magnetic excitations:** Inelastic neutron scattering spectra at zero field and (a)  $T=1.5$  K, (b)  $T=12$  K and (c)  $T=100$  K, taken using  $3 \text{ \AA}$  incident neutrons. The dispersion of the magnetic excitations are more clearly seen in the difference spectra (d)  $\tilde{I}(1.5 \text{ K}) - \tilde{I}(12 \text{ K})$  and (e)  $\tilde{I}(12 \text{ K}) - \tilde{I}(100 \text{ K})$ . (f)  $\tilde{I}(Q, \omega)$  averaged over  $0.3 \text{ \AA}^{-1} < Q < 0.6 \text{ \AA}^{-1}$ . Horizontal bar shows instrument resolution.

The inset of figure 2(a) shows that both the  $\vec{k}_1$  and  $\vec{k}_2$  Bragg peak positions stay fairly constant and remain resolution limited ( $\xi > 50 \text{ \AA}$ ) from  $H=0$  T up to  $H=9$  T, therefore the peak intensity  $I$  is a good measure of the order parameter. Figure 2 shows the temperature dependence of both peak intensities under various external fields. In zero field,  $I(\vec{k}_1)$  develops long range order near  $T=15$  K, has a rounded maximum at  $T=10$  K, and then falls off sharply to a nearly constant non-zero value below  $T=6$  K. The downturn in  $I(\vec{k}_1)$  coincides with a development of long range order associated with  $I(\vec{k}_2)$ , and signals the partial transformation from helical to collinear order. Both peaks exhibit clear thermal irreversibility around  $T_{N2}$  which is consistent with bulk data [8]. The intensity difference between the warming and cooling curves at  $T=7$  K remained unchanged out to a waiting time of 60 minutes, which strongly suggests that the thermal irreversibility results from true hysteresis associated with a first order transition. Previous work has shown that the ratio  $R = I(\vec{k}_1)/I(\vec{k}_2)$  at the lowest temperature is positively correlated with the number of sulphur vacancies in the sample [16]. Our measured value of  $R=0.35(3)$  at  $T=4$  K corresponds well to previous results on sulphur annealed samples.

As the field is raised, we observe a decrease in the onset temperature of the  $\vec{k}_2$  phase and an overall decrease in  $I(\vec{k}_2)$  (Fig. 2(a)). At  $T=4$  K, figure 3(a) shows that higher order peaks belonging to the complex collinear

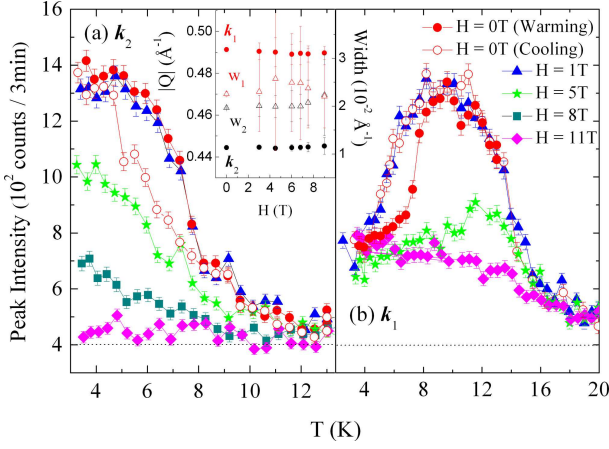


FIG. 2: **Order parameter behavior:** Temperature dependence of the (a)  $\vec{k}_2$  and (b)  $\vec{k}_1$  peak intensities in various external fields taken on BT-7 upon cooling and warming respectively. Both warming and cooling curves are displayed for the  $H=0$  T data to show thermal hysteresis. The dotted line indicates the background (BG) level due to nuclear incoherent scattering. The inset of (a) shows the field dependence of the  $\vec{k}_1$  and  $\vec{k}_2$  peak positions and widths at  $T=4$  K determined by fitting Gaussians to DCS data.

phase all decay with a constant relative intensity before disappearing at a critical field  $H_c(4K) \sim 9$  T. A suppression of both thermal and phonon anomalies at  $T_{N2}$  has also been reported in fields of 7 T [8]. These results show that the long-range ordering temperature of the collinear phase of  $\text{ZnCr}_2\text{S}_4$  is suppressed to zero by a field close to its mean field energy scale  $k_B T_{N2}/g\mu_B \sim 6$  T.

In contrast, the onset temperature of long-range helical order does not change significantly with field (Fig. 2(b)). This is consistent with specific heat measurements which show little change in both the position and magnitude of the anomaly at  $T_{N1}$  up to  $H=7$  T [8]. Therefore unlike the collinear structure, the helical structure is not being suppressed by the applied field. The shape of the  $I(\vec{k}_1)$  versus  $T$  curve does however undergo a qualitative change. At  $H=5$  T,  $I(\vec{k}_1)$  rises below  $T_{N1}$  to a sharp maximum near  $T=13$  K with a diminished amplitude relative to the zero field case, and then decreases gradually upon further cooling. By  $H=11$  T, this maximum completely disappears and we instead observe a monotonic increase of intensity with cooling. The intensity at the lowest temperature, which arises from residual helical regions that are pinned by impurities, is fairly independent of field. We now consider several possibilities to explain the suppression of  $I(\vec{k}_1)$ . (i) If spin anisotropy is present, external fields can exert a torque on magnetically ordered powder grains causing  $\vec{k}_1$  to rotate away from the  $\hat{Q}$  direction. This can be ruled out because no changes were observed in the (220), (311) and (004) nuclear Bragg reflections with field. Moreover, the zero field values of  $I(\vec{k}_1)$  were recovered upon removing the field. (ii) If the magnetic field is large enough to overcome all

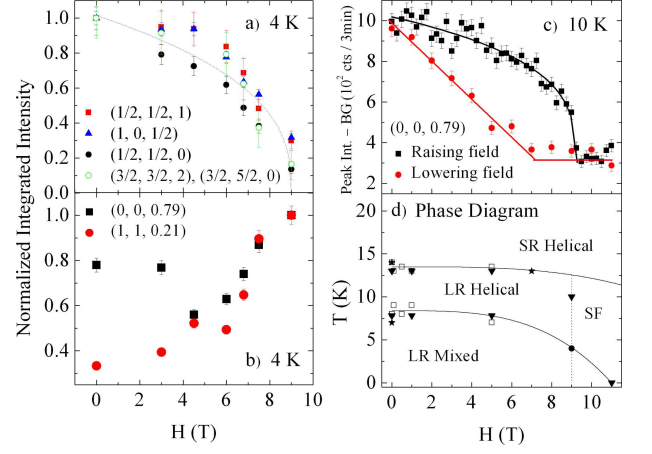


FIG. 3: **Determination of phase diagram:** Magnetic field dependence of the (a)  $\vec{k}_3$ ,  $\vec{k}_2$ ,  $(001)\vec{k}_2$ ,  $(112)\vec{k}_2$  and  $(120)\vec{k}_2$  and (b)  $\vec{k}_1$  and  $(111)^{-\vec{k}_1}$  integrated intensities at 4K normalized by their zero field values and  $H=9$  T values respectively (data from DCS). (c) Background subtracted intensity of the  $\vec{k}_1$  peak taken on BT-7 at  $T=10$  K upon raising followed by lowering the magnetic field. (d)  $H - T$  phase diagram of  $\text{ZnCr}_2\text{S}_4$  constructed using the following data sets: ( $\square$ ) Peak in  $d(\chi T)/dT$ , ( $\star$ ) peak in  $C_p(T)$ , ( $\blacktriangledown$ ) 3 axis neutrons, ( $\bullet$ ) TOF neutrons. Dashed line is the approximate spin-flop (SF) boundary. All lines are guides to the eye.

internal AFM exchange energies, all spins can be made to align with the field. This can again be ruled out because no ferromagnetic contribution was detected atop the nuclear Bragg peaks, and because the bulk magnetization at  $H=11$  T is far below saturation [5]. (iii) The possibility of new magnetic structures induced by the external field is ruled out based on the absence of new diffraction peaks. (iv) The magnetic field may induce a spin-flop transition to an arrangement where spins preserve  $(0\ 0\ 0.79)$  ordering but orient perpendicular to  $\vec{H}$  to take advantage of canting. Since  $\tilde{I}(Q, 0)$  is proportional to the component of the ordered moment perpendicular to  $\hat{Q}$ , this would naturally explain the decrease in  $I(\vec{k}_1)$ .

The spin-flop field  $H_{SF}$  in the purely helical phase lies between 7 T and 9 T as shown in figure 3(c), which is slightly higher than previous estimates ( $H_{SF} \sim 5$  T) based on single crystal magnetization data [20]. Upon entering the mixed phase,  $I(\vec{k}_1)$  becomes rather insensitive to field as shown in figure 2(b). However a general positive correlation is evidenced in figure 3(c), which suggests that an external field stabilizes the helical structure over the collinear structure. The fact that the relative intensity of the  $\vec{k}_1$  and  $(111)^{-\vec{k}_1}$  reflections does not stay constant is further support for a spin-flop transition. The magnetic phase boundaries deduced from our neutron scattering experiments, along with complementary dc-susceptibility and specific heat measurements [8] are summarized in figure 3(d).

Figures 4(a)-(c) show  $\tilde{I}(Q, \omega)$  spectra at  $T=4$  K in

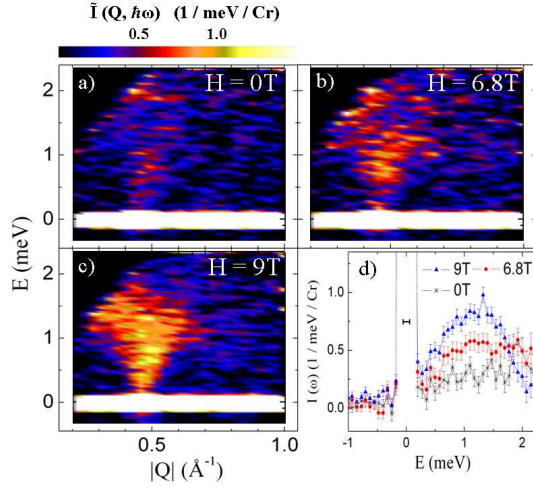


FIG. 4: **High field magnetic excitations:** High resolution inelastic neutron scattering spectra at  $T=4$  K and (a)  $H=0$  T, (b)  $H=6.8$  T and (c)  $H=9$  T, taken using  $4.8$  Å incident neutrons. The background from the empty cryostat has been subtracted off. (d)  $\bar{I}(Q, \omega)$  averaged over  $0.3 \text{ Å}^{-1} < Q < 0.6 \text{ Å}^{-1}$ . Horizontal bar shows instrument resolution.

three external magnetic fields. These data employed  $4.8$  Å incident neutrons which gives a reduced dynamic range relative to Fig. 1. At  $H=0$  T, weak low energy scattering from residual helical ordered regions of the sample is again visible. As the field is increased, this envelope of spin wave dispersion fills in with inelastic intensity. By  $H=H_c$  an excitation spectrum characteristic of the purely helical ordered phase (Fig. 1(b)) is recovered. Indeed, the total fluctuating moment at  $H=9$  T obtained by integrating over the region  $\hbar\omega \in [0.15, 2] \text{ meV}$  and  $Q \in [0.2, 0.8] \text{ Å}^{-1}$  is  $\langle \delta m \rangle^2 = 1.1(3)/\text{Cr}$ , comparable to the zero field value measured in the purely helical phase at

$T=12$  K. The  $Q$ -averaged scattering (Fig. 4(d)) shows that the magnetic field induces a shift of high energy spectral weight down into a  $1$  meV maximum, in accordance with a conversion from collinear to helical magnetic order. Since the magnetic inelastic scattering cross section is proportional to the component of the fluctuating moment perpendicular to  $\hat{Q}$ , strong inelastic scattering together with a low value of  $I(\vec{k}_1)$  at  $H=9$  T is fully consistent with the system being in a spin-flopped phase.

In summary, we have observed a rare field-induced commensurate to incommensurate magnetic ordering transition [21] in bond frustrated  $\text{ZnCr}_2\text{S}_4$ , with a concomitant closing of a spin wave gap. The phase boundary is fully consistent with that derived from structural measurements, which indicates strong spin-phonon coupling in this system. Recent theoretical work has shown that spiral magnets, which break both time reversal and inversion symmetry, permit a permanent electric dipole moment  $\vec{P} \propto \vec{e}_3 \times \vec{k}$  where  $\vec{e}_3$  is the spin rotation axis and  $\vec{k}$  the ordering wave vector [22]. While the zero-field helical phase of  $\text{ZnCr}_2\text{S}_4$  does not permit a finite  $\vec{P}$  since  $\vec{e}_3 \parallel \vec{k}_1$ , it would be interesting to search for an electric polarization in the spin-flopped phase above  $H_{SF}$  which does permit one. Further progress towards refining the low temperature magnetic structure in a field will require neutron scattering experiments on single crystalline samples in both vertical and horizontal field magnets.

We thank L. Li, K. Holman and Z. Tan for help with sample characterization. We also acknowledge useful discussions with M. J. Bhaseen, S. Sondhi, D. Huse and C. Broholm. The identification of any commercial product or trade name does not imply endorsement or recommendation by the National Institute of Standards and Technology.

- 
- [1] A.P. Ramirez, in *Handbook of Magnetic Materials* (North-Holland, Amsterdam, 2001), Vol. 13, Chap. 4, p. 423.
  - [2] S.-H. Lee *et al.*, *Nature (London)* **418**, 856 (2002).
  - [3] S.-H. Lee *et al.*, *Phys. Rev. Lett.* **86**, 5554 (2001).
  - [4] J.-H. Chung *et al.*, *Phys. Rev. Lett.* **95**, 247204 (2005).
  - [5] H. Ueda *et al.*, *Phys. Rev.* **B73**, 094415 (2006).
  - [6] M. Matsuda *et al.*, *Nature Phys.* **3**, 397 (2007).
  - [7] N. Menyuk *et al.*, *J. Appl. Phys.* **37**, 1387 (1966); K. Baltzer *et al.*, *Phys. Rev.* **151**, 367 (1966).
  - [8] J. Hemberger *et al.*, *Phys. Rev. Lett.* **97**, 087204 (2006).
  - [9] T. Rudolf *et al.*, *Phys. Rev.* **B75**, 052410 (2007).
  - [10] V. Tsurkan *et al.*, *Phys. Rev.* **B73**, 224442 (2006).
  - [11] M. Hidaka *et al.*, *Phys. Stat. Sol. (b)* **236**, 9 (2003).
  - [12] M. Hidaka *et al.*, *Phys. Stat. Sol. (b)* **236**, 209 (2003).
  - [13] S.-W. Cheong *et al.*, *Nature Mater.* **6**, 13 (2007).
  - [14] J. Hemberger *et al.*, *Nature (London)* **434**, 364 (2005); S. Weber *et al.*, *Phys. Rev. Lett.* **96**, 157202 (2006).
  - [15] V. Gnezdilov *et al.*, *Phys. Rev.* **B84**, 045106 (2011).
  - [16] M. Hamedoun *et al.*, *J. Phys. C: Solid State Phys.* **19**, 1783 (1986).
  - [17] J. W. Lynn *et al.*, *J. Research NIST* **117**, 61 (2012).
  - [18] We use the notation of S.W. Lovesey, *Theory of Neutron Scattering from Condensed Matter*, vol. 2 (Clarendon Press, Oxford, 1984).
  - [19] S.-H. Lee *et al.*, *Phys. Rev. Lett.* **84**, 3718 (2000).
  - [20] M. Hamedoun *et al.*, *J. Phys. C: Solid State Phys.* **19**, 1801 (1986).
  - [21] A. Zheludev *et al.*, *Phys. Rev. Lett.* **78**, 4857 (1997).
  - [22] M. Mostovoy, *Phys. Rev. Lett.* **96**, 067601 (2006).